

Bounds from LEP on unparticle interactions with electroweak bosons.

Scott Kathrein,^{*} Simon Knapen,[†] and Matthew J. Strassler[‡]

*Department of Physics and Astronomy,
 Rutgers University, Piscataway, NJ 08854*

A conformally invariant hidden sector is considered, with a scalar operator \mathcal{O} of low dimension that couples to the electro-weak gauge bosons of the Standard Model, via terms such as $F^{\mu\nu}F_{\mu\nu}\mathcal{O}$. By examining single photon production at LEP, we bound the strength of these interactions. We apply our results, along with those of Delgado and Strassler [1] and of Caracciolo and Rychkov [2], to improve the bound on 4γ production through “unparticle self-interactions”, as proposed by Feng et al. [3]. We find the maximum allowable cross-section is of order a few tens of femtobarns at the 14 TeV LHC, and lies well below 1 fb for a wide range of parameters.

I. INTRODUCTION

A “hidden” sector of light particles, none of which carry standard model quantum numbers, is still allowed by experiment. Neither direct searches, nor indirect tests of the standard model, nor cosmology or astrophysics can exclude this possibility. If the coupling of such a sector to our own is purely through gravitation, constraints are extremely weak. But if additional interactions, with characteristic energy scales far below the Planck scale, are present, then it is possible to obtain some correlated constraints on the strength of those interactions and the contents of the hidden sector.

Since the contents of such a sector are all neutral and may all be stable or metastable, production of anything in that sector may generally be invisible. In such a case, constraints may be obtained at a wide range of particle colliders, using their searches for unexplained

^{*}Electronic address: kathrein@physics.rutgers.edu

[†]Electronic address: knapen@physics.rutgers.edu

[‡]Electronic address: strassler@physics.rutgers.edu

sources of missing momentum. At a hadron collider, the typical search is for a jet or a photon plus missing transverse momentum. At an electron-positron collider, a powerful constraint may be obtained from searches for “photon-plus-nothing” — events in which a photon is observed whose momentum is not balanced against any visible object. Since the collision energy and momentum are known at a lepton collider, the four-momentum of the missing object, and its square, the “missing mass,” may be reconstructed. The events are very clean and easy to interpret, though a background from $e^+e^- \rightarrow \gamma\nu\bar{\nu}$, where the neutrinos may or may not originate from an on-shell Z^0 , must be removed.

In this article, we consider constraints on hidden sectors from photon-plus-nothing searches at the Large Electron-Positron (LEP) collider in its two stages, LEP I (at the Z boson peak) and LEP II (at center-of-mass energies up to 209 GeV). Our focus here will be on exactly or approximately conformal hidden sectors, now often called “unparticle” sectors [4]. We will obtain constraints on couplings of $SU(2) \times U(1)$ gauge bosons to low-dimension scalar operators in such sectors. We only consider operators with dimension less than 2. (For $\Delta > 2$, operator renormalizations become necessary and the calculations become sensitive to the ultraviolet, leaving them less predictive. Note also that unitarity requires $\Delta \geq 1$.)

As an application of our results, we will combine them with the work of [1] and [2] to obtain limits on the process $gg \rightarrow \gamma\gamma\gamma\gamma$, highlighted in [3] as a possible source of a large effect of an unparticle sector. We will see that where qualitatively new constraints can be obtained, the allowed signals must lie below 5 fb, even at a 14 TeV collider.

In section 2, we will discuss the general theoretical background and calculations needed for this paper. In section 3, we will obtain bounds from LEP results. Finally, we will apply these bounds in the particular case of four-photon production at the LHC.

II. NATURE OF THE CFT COUPLING

In what follows, we imagine that, through new physics somewhat above the TeV scale, a hidden conformal (unparticle) sector is coupled to the standard model gauge bosons. (Couplings to fermions risk flavor-changing neutral currents, unless they occur through conserved currents of dimension 3, in which case contact terms generally dominate [5].) We assume the following Lagrangian, where a scalar primary operator \mathcal{O} of the conformal

sector couples to the electroweak gauge fields.

$$\delta\mathcal{L} = \frac{\lambda_1}{\Lambda_1^\Delta} B^{\mu\nu} B_{\mu\nu} \mathcal{O} + \frac{\lambda_2}{\Lambda_2^\Delta} W_a^{\mu\nu} W_{\mu\nu}^a \mathcal{O}. \quad (\text{II.1})$$

Here, $|\lambda_1| = |\lambda_2| = 1$ and Λ_1 and Λ_2 are real and positive. The two conformal operators in this expression are assumed to be the same, with scaling dimension Δ ; we consider only $2 \geq \Delta \geq 1$. As is the standard operating procedure in the literature on scalar unparticle sectors, we ignore serious subtleties involving the generation of the operator $|\mathcal{O}|^2$ through quantum effects, assuming that (as for the Higgs mass operator) the coefficient of the operator is suppressed through an unspecified mechanism. Examples of possible mechanisms include supersymmetry; see for example [6].

After electroweak symmetry breaking mixes the B and the W^3 to form the photon and the Z^0 , the Lagrangian contains the terms

$$\delta\mathcal{L}_{\gamma\gamma} = 2(c_\theta^2 \frac{\lambda_1}{\Lambda_1^\Delta} + s_\theta^2 \frac{\lambda_2}{\Lambda_2^\Delta})(\partial_\mu A_\nu \partial^\mu A^\nu - \partial_\mu A_\nu \partial^\nu A^\mu) \mathcal{O} \quad (\text{II.2})$$

$$\delta\mathcal{L}_{Z\gamma} = 4c_\theta s_\theta (\frac{\lambda_2}{\Lambda_2^\Delta} - \frac{\lambda_1}{\Lambda_1^\Delta})(\partial_\mu A_\nu \partial^\mu Z^\nu - \partial_\mu A_\nu \partial^\nu Z^\mu) \mathcal{O} \quad (\text{II.3})$$

$$\delta\mathcal{L}_{ZZ} = 2(s_\theta^2 \frac{\lambda_1}{\Lambda_1^\Delta} + c_\theta^2 \frac{\lambda_2}{\Lambda_2^\Delta})(\partial_\mu Z_\nu \partial^\mu Z^\nu - \partial_\mu Z_\nu \partial^\nu Z^\mu) \mathcal{O} \quad (\text{II.4})$$

$$\delta\mathcal{L}_{WW} = 2\frac{\lambda_2}{\Lambda_2^\Delta}(\partial_\mu W_\nu^\pm \partial^\mu W^{\pm\nu} - \partial_\mu W_\nu^\pm \partial^\nu W^{\pm\mu}) \mathcal{O}, \quad (\text{II.5})$$

where $c_\theta \equiv \cos(\theta_w)$ and $s_\theta \equiv \sin(\theta_w)$. The following definitions will simplify formulae

$$\frac{\lambda_\gamma}{\Lambda_\gamma^\Delta} \equiv c_\theta^2 \frac{\lambda_1}{\Lambda_1^\Delta} + s_\theta^2 \frac{\lambda_2}{\Lambda_2^\Delta} \quad (\text{II.6})$$

$$\frac{\lambda_Z}{\Lambda_Z^\Delta} \equiv \frac{\lambda_2}{\Lambda_2^\Delta} - \frac{\lambda_1}{\Lambda_1^\Delta} \quad (\text{II.7})$$

with $|\lambda_\gamma| = |\lambda_Z| = 1$ and Λ_γ and Λ_Z real and positive. For the present article the most interesting interactions will be those involving the photon. The photon–photon–unparticle vertex, and the photon– Z^0 –unparticle vertex, lead to vertices with Feynman rules [3, 7]

$$\gamma\gamma\mathcal{O} \rightarrow -4i \frac{\lambda_\gamma}{\Lambda_\gamma^\Delta} (g^{\mu_1\mu_2} k_1 \cdot k_2 - k_1^{\mu_2} k_2^{\mu_1}) \quad (\text{II.8})$$

$$Z\gamma\mathcal{O} \rightarrow -4ic_\theta s_\theta \frac{\lambda_Z}{\Lambda_Z^\Delta} (g^{\mu_1\mu_2} k_1 \cdot k_2 - k_1^{\mu_2} k_2^{\mu_1}). \quad (\text{II.9})$$

In Sec. V, we will assume that the gluons couple to the unparticle sector as well. We will rename \mathcal{O} and Δ as \mathcal{O}_γ and Δ_γ , and permit the gluons to couple to an operator \mathcal{O}_g

$$\delta\mathcal{L} = \frac{\lambda_g}{\Lambda_g^\Delta} G_{\mu\nu}^a G_a^{\mu\nu} \mathcal{O}_g \quad (\text{II.10})$$

$$= 2 \frac{\lambda_g}{\Lambda_g^\Delta} (\partial_\mu G_\nu^a \partial^\mu G_a^\nu - \partial_\mu G_\nu^a \partial^\nu G_a^\mu) \mathcal{O}_g. \quad (\text{II.11})$$

Here, \mathcal{O}_g (and Δ_g) may or may not be the same as \mathcal{O}_γ (and Δ_γ). (Note that [3], in considering four photon production at the Tevatron and LHC, assumed $\mathcal{O}_g = \mathcal{O}_\gamma$.) This Lagrangian yields the vertex

$$gg\mathcal{O}_g \rightarrow -4i \frac{\lambda_g}{\Lambda_g^\Delta} (g^{\mu_1\mu_2} k_1 \cdot k_2 - k_1^{\mu_2} k_2^{\mu_1}) \delta_{a_1}^{a_2}. \quad (\text{II.12})$$

III. CROSS SECTION

The amplitude for $e^+e^- \rightarrow \{\gamma \text{ or } Z^0\} \rightarrow \gamma\mathcal{O}$ at tree level (figure 1) is

$$\overline{\sum} |M|^2 = A(\Lambda) \frac{e^2}{s} (t^2 + u^2) \quad (\text{III.1})$$

$$(\text{III.2})$$

where

$$A(\Lambda) \equiv \left(A_Z \frac{1}{\Lambda_Z^{2\Delta}} + A_\gamma \frac{1}{\Lambda_\gamma^{2\Delta}} + A_{Z\gamma} \frac{1}{\Lambda_Z^\Delta \Lambda_\gamma^\Delta} \right) \quad (\text{III.3})$$

$$A_Z \equiv \left(\frac{1}{2} - 2s_\theta^2 + 4s_\theta^4 \right) \left(\frac{s^2}{(s - m_Z^2)^2 + m_Z^2 \Gamma_Z^2} \right) \quad (\text{III.4})$$

$$A_\gamma \equiv 4 \quad (\text{III.5})$$

$$A_{Z\gamma} \equiv 2(1 - 4s_\theta^2) \left(\frac{(s - m_Z^2) \cos(\delta) - m_Z \Gamma_Z \sin(\delta)}{(s - m_Z^2)^2 + m_Z^2 \Gamma_Z^2} \right) s. \quad (\text{III.6})$$

Here δ is the relative phase difference between the two diagrams in 1(a) and 1(b), originally parametrized by λ_γ and λ_Z . The result for A_γ matches [8] appropriately in the $\Delta \rightarrow 1$ limit.

The differential cross section is calculated with respect to the Mandelstam variables t and u , as well as with respect to $\cos \theta$ and q , with q the energy of the final state photon.

$$\frac{d^2\sigma}{dt du} = \frac{(4\pi)^{1-2\Delta}}{4\Gamma(\Delta-1)\Gamma(\Delta)} A(\Lambda) e^2 \frac{(t^2 + u^2)(s + t + u)^{\Delta-2}}{s^3} \quad (\text{III.7})$$

$$\frac{d^2\sigma}{dq d\cos\theta} = \frac{(4\pi)^{1-2\Delta}}{\Gamma(\Delta-1)\Gamma(\Delta)} A(\Lambda) e^2 q^3 s^{\Delta-3} \left(1 - 2\frac{q}{\sqrt{s}}\right)^{\Delta-2} (1 + \cos^2\theta) \quad (\text{III.8})$$

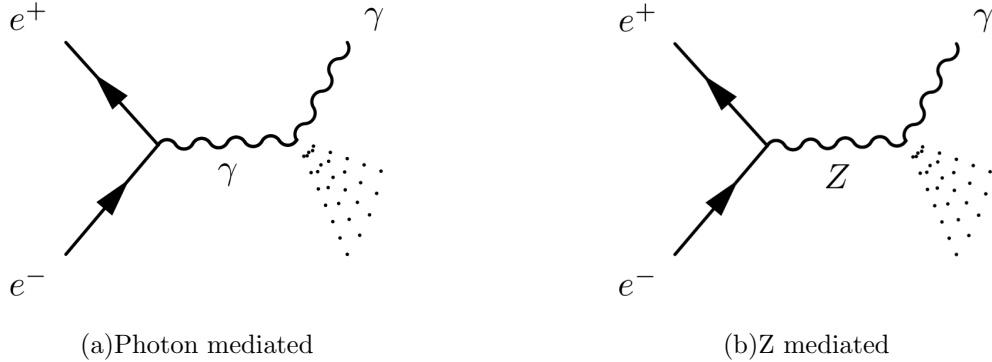


FIG. 1: Feynman diagrams for production of hidden states in the LEP collider. The dots represent states in the conformal hidden sector.

The latter result is most suitable for numerical integration to compare to experiments with lepton colliders.

At the peak of the Z^0 resonance, $|A_Z| \sim 85|A_\gamma + A_{Z\gamma}|$, for $\delta = 0$ or $\delta = \pi$. This ratio becomes the smallest for $\delta = 3\pi/2$, where $|A_Z| \sim 35|A_\gamma + A_{Z\gamma}|$. From LEP I data at the Z^0 resonance, we mainly obtain a bound of Λ_Z alone. At LEP II energies, near 200 GeV, $|A_\gamma| \sim 7|A_Z + A_{Z\gamma}|$ for $\delta = 0$, up to a maximum of $|A_\gamma| \sim 19|A_Z + A_{Z\gamma}|$ for $\delta = \pi$, and thus we obtain a limit mainly on Λ_γ .

IV. BOUNDS FROM LEP DATA

A. From LEP I data

During the first run of the LEP experiment, data was collected at the Z-resonance. Unparticle production is therefore dominated by the A_Z term (see Eq. III.3), as was argued in the previous paragraph. To obtain a worst case bound on Λ_Z , we will neglect contributions from the photon channel.¹ This bound could be only slightly improved by incorporating the data from LEP II.

As can be seen from the energy distribution of the single photon in formula III.8, unparticles tend to produce very hard photons for values of Δ less than two. The Standard

¹ Strictly speaking, if the phase δ is such that interference is maximally destructive, including the photon channel can decrease the signal by up to 1%. But this is less than other systematic errors discussed in IV C, so we neglect it.

Model background for this signal on the other hand is only of order 0.5-1 events. To obtain optimal sensitivity for our bounds we require the photon energy to be larger than a certain minimum energy, E_{cut} , which is determined by optimizing the sensitivity for the bound on Λ_Z . More details on the energy cuts can be found in appendix C. None of the four LEP I detectors observed events that pass our energy cuts [9–12].

Combining (as described in the appendix) the available data from all four experiments we establish a 95% confidence level (CL) bound on Λ_Z , following [13]. Our bounds are displayed in table I. A plot of the allowed regions for Λ_2 and Λ_1 , the couplings to the $SU(2) \times U(1)$ bosons, is also given in figure 3. For this plot, the entire matrix element was taken into account.

The value we give for Λ_Z when $\Delta \rightarrow 1$ is consistent with the known branching fraction for $Z \rightarrow \gamma + X$, where X is a very light new invisible particle and $E_\gamma \sim 45$ GeV. The partial width for this process would be

$$\Gamma = \frac{c_\theta^2 s_\theta^2 M_Z^3}{6\pi \Lambda_Z^2}. \quad (\text{IV.1})$$

Since no 45 GeV photons plus missing energy were observed in any of the four LEP experiments, one can obtain a model-independent 95% CL bound on the branching ratio. The best such published bound, 1.1×10^{-6} , was obtained by the L3 experiment [10], and this can be converted to $\Lambda_Z > 51$ TeV with 95% CL. The bound in our table above is consistent with this, though somewhat stronger since we combine all four LEP I experiments in our calculation.

B. From LEP II data

The second run of LEP scanned center of mass energies from 130 GeV to 209 GeV. Since the cross section III.8 grows with \sqrt{s} , the highest collider energies will give us the best bounds. The dominant mode of unparticle production at these energies is via the photon channel, and interference effects are small, so we obtain a worst case bound on Λ_γ by neglecting contribution from the Z channel.

As mentioned above, the best bounds on Λ_γ can be obtained from the highest energies at LEP II. Our bounds below therefore take account only of data from energy in the range 183-209 GeV. In particular, DELPHI [14], ALEPH [15], and L3 [16] published results for \sqrt{s} between 183 GeV and 209 GeV, while OPAL [17] did not publish a result above 189 GeV.

If one accounted for the results at lower collider energies, it would be possible to extract a bound that is slightly better than ours.

Since the collider energy was changed over time, the data in [14–17] are given not in terms of the photon energy itself but in terms of the “missing mass”, the mass that an invisible particle would have had if it were recoiling from the observed photon. For low Δ , the signal is peaked in the low missing mass region,² while for higher Δ , the signal is rather flat. Since the standard model background is smallest in the low missing-mass region, far from the $Z \rightarrow \nu\bar{\nu}$ peak, integrating the signal from zero missing mass up to some maximum missing-mass M_{cut} yields the best bounds. The selection of M_{cut} for each Δ , and other details of our analysis, are described in appendix C. OPAL, ALEPH and in particular DELPHI detected several events that pass our energy cuts. The bounds we obtain are found in table I. The allowed regions for Λ_2 and Λ_1 (the couplings to the $SU(2) \times U(1)$ bosons) are given in figure 4; here the entire matrix element including the Z contribution is taken into account.

Finally, we wish to note that there are ambiguities regarding the interpretation of certain published plots which affect the analyses, and require us to make certain assumptions. A key ambiguity regarding our analysis revolves around the result of the DELPHI experiment. (At DELPHI, as with the other experiments, we only use data from approximately 45 to 135 degrees; see appendix C.) In the bin at zero missing mass, there are 7 events, above one expected in background. This bin was used as an underflow, and at least 6 of the events³ are from “photons” with energy larger than half the beam energy, giving a negative apparent missing mass, which is not consistent with our signal. We therefore view the interpretation of one unexplained event in this bin as ambiguous. There are several choices, including discarding this bin as having large background, discarding the 7th event in the bin as being more plausibly background than signal, discarding the DELPHI data completely, etc.

Our table above reflects the most liberal (but in our view, also the most plausible) assumption that the seventh event in the zero-missing-mass bin is, like the other six, from a background source. It is likely that this could be shown to be the case with sufficient information about the DELPHI data. If instead we treat the seventh event as a potential signal, the effect on our bounds is substantial in the regime where Δ is small, on the order

² $\Delta=1$ corresponds to a massless invisible scalar particle.

³ We are very grateful to C. Mateuzzi of DELPHI for providing us with considerable information about these events.

| Δ | Λ_Z | Λ_γ |
|----------|-------------|------------------|
| 1 | 69.5 | 25.2 |
| 1.01 | 59.0 | 23.0 |
| 1.05 | 40.7 | 13.2 |
| 1.1 | 26.6 | 8.0 |
| 1.2 | 12.7 | 3.6 |
| 1.3 | 6.8 | 2.0 |
| 1.4 | 4.0 | 1.2 |
| 1.5 | 2.5 | 0.79 |
| 1.6 | 1.6 | 0.57 |
| 1.7 | 1.1 | 0.41 |
| 1.8 | 0.80 | 0.30 |
| 1.9 | 0.60 | 0.24 |
| 2 | 0.46 | 0.19 |

TABLE I: 95 % confidence level lower bounds on the given scales, in TeV, from LEP data. For bounds on Λ_1 and Λ_2 , see the figures in Appendix A.

of 20% in Λ_γ .

C. Error Estimate

The largest uncertainty in both the LEP I and the LEP II analyses (other than the ambiguities in the LEP II data described above) is due to the systematic errors in manually reading the backgrounds from the graphs. However, in the case of LEP I, this error only contributes in the calculation of the cuts, as no events are found in the signal region [13]. Furthermore we find that the bounds are not very sensitive to cuts, and the error due to the background only contributes a few percent to the total error on the bounds. When accounting for experimental uncertainties we can estimate the total uncertainty on the bounds to be within 5%.

For LEP II, the systematic uncertainty from reading backgrounds from the plots is significantly larger. Moreover the bounds do depend directly on the background in this case,

although the dependence is very mild. The total uncertainties on the bound on Λ_γ are estimated to be smaller than 10%. In these estimates we ignore the much larger systematic uncertainties that arise from the ambiguities described above in the interpretation of the published data.

V. FOUR PHOTON SIGNALS

Multi-point correlation functions (sometimes called “unparticle self-interactions”) for the conformal operators \mathcal{O} have been proposed as a possible source at the LHC of very large new-physics signals — including four-photon signals as large as 10 nb [3]. But as shown in [1], CDF limits on signals that give a jet plus missing transverse momentum (MET), and general considerations of unitarity and self-consistency, strongly constrain such processes, to a few fb in some regimes (including those considered in [3]) and a few pb in some other regimes. The results of the current paper, combined with work of [2], allow us to improve constraints by several orders of magnitude. Limits on the maximum cross-section for $gg \rightarrow 4\gamma$ at a 14 TeV LHC are given in table II. In this table, we assume that the standard model gauge bosons couple to operators \mathcal{O}_g and \mathcal{O}_γ , with dimensions Δ_g and Δ_γ , as described in Sec. II.

Before explaining how we obtained these results, let us make a couple of brief comments. Compared to [1], our new bounds for $\Delta_\gamma < 1.7$ are far stronger, especially for small Δ_γ , by as many as five orders of magnitude. We can see that bounds are below 5 fb for $\Delta_\gamma < 1.7$. For $\Delta_\gamma > 1.7$ we must rely on the methods of [1] (extended to 14 TeV), obtaining constraints of a few tens of fbs or less at low to moderate Δ_g . We should note also that the bounds at low Δ_g are obtained from a CDF jet-plus-MET measurement [18] that uses only 1.1 inverse fb of data, much less than the total Tevatron data set.

A. Obtaining the bounds

In general, the cross section for $gg \rightarrow 4\gamma$ is proportional to $C_3^2 \Lambda_g^{-2\Delta_g} \Lambda_\gamma^{-4\Delta_\gamma} \hat{s}^{\Delta_g+2\Delta_\gamma-1}$, where C_3 is the coefficient of the three-point function $\langle \mathcal{O}_g \mathcal{O}_\gamma \mathcal{O}_\gamma \rangle$, and the scales $\Lambda_g, \Lambda_\gamma$ and dimensions Δ_g, Δ_γ are as defined in section II. (In [3] both the gluons and the photons are assumed to couple to the same operator in the conformal sector, but this is an unnecessary assumption.) The potentially enormous cross-sections suggested by [3] arise from the rapid

growth with \hat{s} ; even strong limits on 4γ production at the Tevatron naively allow very large LHC signals. But [3] did not consider unitarity, or direct and indirect constraints on Λ_g , Λ_γ and C_3 . In [1], experimental and theoretical bounds on Λ_g were found (table III), along with a simple unitarity argument that eliminated the possibility of very large cross-sections. In the current article we have found experimental bounds on Λ_γ , which (as described below) we may supplement with theoretical bounds. And recently, unitarity constraints on C_3 , from internal consistency arguments of the conformal field theory, were obtained in [2] for $\Delta_\gamma < 1.7$ and any Δ_g . We now explain how these bounds are obtained and combined together into table II.

In the regime $\Delta_\gamma > 1.7$, indicated by numbers in italics in the table, the constraints obtained in [1] are extended to a 14 TeV LHC, using bounds on Λ_g only. Direct experimental bounds on Λ_g arise because the gluon-gluon-unparticle interaction can generate a large jet-plus-MET signature [1]. Limits from CDF [18] using 1.1 fb^{-1} of data (unfortunately not

| $\Delta_g \setminus \Delta_\gamma$ | 1.05 | 1.1 | 1.2 | 1.3 | 1.4 | 1.5 | 1.6 | 1.7 | 1.8 | 1.9 | 2.0 |
|------------------------------------|--|--|--|--------------|-------------|-------------|-------------|-------------|------------|------------|-------------|
| 1.05 | 2.7×10^{-6} | 2.7×10^{-5} | 4.8×10^{-4} | 0.010 | 0.093 | 0.62 | 1.1 | 1.7 | <i>3.8</i> | <i>2.3</i> | <i>1.4</i> |
| 1.1 | 5.1×10^{-6} | 5.2×10^{-5} | 6.7×10^{-4} | 0.014 | 0.13 | 0.89 | 1.4 | 1.6 | <i>9.6</i> | <i>5.9</i> | <i>3.7</i> |
| 1.2 | 1.5×10^{-5} | 1.4×10^{-4} | 1.3×10^{-3} | 0.023 | 0.37 | 2.4 | 2.3 | 1.7 | <i>2.3</i> | <i>1.4</i> | <i>7.1</i> |
| 1.3 | 3.7×10^{-5} | 2.8×10^{-4} | 3.2×10^{-3} | 0.031 | 0.33 | 1.7 | 1.2 | 0.91 | <i>16.</i> | <i>9.3</i> | <i>5.4</i> |
| 1.4 | 3.3×10^{-5} | 2.5×10^{-4} | 2.3×10^{-3} | 0.023 | 0.24 | 1.2 | 0.73 | 0.56 | <i>12.</i> | <i>7.1</i> | <i>4.5</i> |
| 1.5 | 3.6×10^{-5} | 2.4×10^{-4} | 2.8×10^{-3} | 0.025 | 0.19 | 0.78 | 0.57 | 0.37 | <i>9.3</i> | <i>5.4</i> | <i>3.2</i> |
| 1.6 | 3.6×10^{-5} | 2.6×10^{-4} | 2.3×10^{-3} | 0.021 | 0.16 | 0.55 | 0.48 | 0.31 | <i>7.1</i> | <i>4.7</i> | <i>2.5</i> |
| 1.7 | 4.7×10^{-5} | 2.9×10^{-4} | 2.7×10^{-3} | 0.024 | 0.16 | 0.50 | 0.35 | 0.26 | <i>5.4</i> | <i>3.2</i> | <i>2.0</i> |
| 1.8 | 4.4×10^{-5} | 2.2×10^{-4} | 1.7×10^{-3} | 0.022 | 0.20 | 0.38 | 0.32 | 0.23 | <i>4.2</i> | <i>2.5</i> | <i>1.5</i> |
| 1.9 | 3.4×10^{-5} | 1.6×10^{-4} | 1.5×10^{-3} | 0.014 | 0.15 | 0.36 | 0.29 | 0.23 | <i>3.2</i> | <i>2.0</i> | <i>1.2</i> |
| 2.0 | 2.7×10^{-5} | 1.3×10^{-4} | 8.7×10^{-4} | 0.013 | 0.14 | 0.35 | 0.31 | 0.24 | <i>2.5</i> | <i>1.5</i> | <i>0.96</i> |

TABLE II: Bounds on 4 photon production, in fb. Values in regular font are obtained using only experimental limits on Λ_g and Λ_γ ; see also Appendix B. Values in boldface are obtained from experimental and unitarity bounds, or unitarity bounds only, on these scales. The values in italics are calculated using the unitarity argument of [1].

| Δ_g | Λ_g (TeV) | Δ_g | Λ_g (TeV) |
|------------|-------------------|------------|-------------------|
| 1.05 | 9.19 | 1.55 | 1.08 |
| 1.10 | 6.82 | 1.60 | 0.94 |
| 1.15 | 5.18 | 1.65 | 0.82 |
| 1.20 | 4.03 | 1.70 | 0.73 |
| 1.25 | 3.19 | 1.75 | 0.64 |
| 1.30 | 2.58 | 1.80 | 0.58 |
| 1.35 | 2.11 | 1.85 | 0.52 |
| 1.40 | 1.75 | 1.90 | 0.47 |
| 1.45 | 1.48 | 1.95 | 0.43 |
| 1.50 | 1.26 | | |

TABLE III: Lower bounds (quoting and extending the results of [1]) on the interaction scale Λ_g as a function of Δ_g , using only constraints from jet-plus-MET studies at CDF [18]. The unitarity considerations also discussed in [1] are not applied here.

yet updated for the current, much larger, Tevatron data sets) were obtained in [1], and are extended in table III. These bounds are powerful at small Δ_g .

A theoretical bound on Λ_g is obtained as follows. A coupling of gluons of the form $G^2\mathcal{O}$ corrects the $\langle\mathcal{O}(p)\mathcal{O}(-p)\rangle$ two-point function by a computable amount. Once this correction becomes large enough that the two-point function is no longer of its conformal form, the assumptions that undergird the conformal computation break down: either conformal invariance fails or the pointlike coupling $G^2\mathcal{O}$ develops a form factor, in both cases acting to reduce the cross-section. As emphasized in [1], the dominant cross-section for $gg \rightarrow 4\gamma$ is at very large \hat{s} , because $d\sigma/d\hat{s}$ initially grows with \hat{s} even after the falling parton distribution functions are accounted for, shrinking only at multi-TeV energies. Thus for the cross-section to be correctly computed, the energy at which conformal invariance breaks down must be somewhat larger than the energy $\sqrt{\hat{s}_{max}}$ at which the cross-section peaks. This constraint was computed for a 10 TeV LHC in [1]. Here we use the self-consistency constraints for a 14 TeV LHC.

For smaller Δ_γ , we need bounds on both scales. We obtain constraints on Λ_γ using our direct LEP II bounds on this quantity at small Δ_γ from table I, and using unitarity

considerations at large Δ_γ . Since there are four photons in the final state, we require consistency for all diphoton invariant masses up to $\sqrt{\hat{s}_{max}}/2$, noting (see below) that the dominant cross-section arises where both photon pairs have invariant mass of this order.

For C_3 , constraints can be read off from Figures 1 and 2 of [2]. The absence of constraints for $\Delta_\gamma > 1.7$ may be purely technical, and perhaps other bounds may be obtained in this region. However, we only use the results of [2] as they currently stand.

We now combine these (for $\Delta_\gamma < 1.7$) with an overall bound on the squared matrix element, integrated over phase space, allowing us to obtain the results in table II. In principle we could compute the exact cross-section (for a given C_3 , Λ_g and Λ_γ) but it is already sufficient, as we will see, to make a rough estimate that bounds the true cross-section from above.⁴ Since

$$\int d[\text{Phase Space}] |\mathcal{M}|^2 < |\mathcal{M}^2|_{max} \int d[\text{Phase Space}] , \quad (\text{V.1})$$

and the phase space for four identical massless particles of total energy $\sqrt{\hat{s}}$ can be computed

$$\int d[\text{Phase Space}] = \frac{1}{4!} \frac{\hat{s}^2}{2^{13} 3 \pi^5} \quad (\text{V.2})$$

we only need to bound the squared matrix element. We do this by bounding \mathcal{M} itself, which contains three diagrams related by permutation of the final state photons, as shown in figure 2. Let us consider the first diagram, where photons couple to the hidden sector in pairs 1,2 and 3,4. (The other diagrams give the same bound.) The diagram factors into a standard model piece and a hidden sector piece. The standard model piece can be bounded directly. The kinematic factor from the two gluons can be treated exactly, but for the photons, with momenta p_1, p_2, p_3, p_4 , we make an approximation. The two photon pairs each have a kinematic factor from $F^{\mu\nu} F_{\mu\nu}$ which satisfies

$$|\epsilon_i \cdot \epsilon_j p_i \cdot p_j - \epsilon_i \cdot p_j p_i \cdot \epsilon_j| < p_i \cdot p_j = m_{ij}/2 , \quad (\text{V.3})$$

where m_{ij} is the invariant mass of photons i, j . Then we note that $m_{12}m_{34}$ times the hidden sector matrix element can also be bounded; it is maximized where $m_{12} = m_{34} = \sqrt{\hat{s}}/2$. Armed with this bound on each of the three terms in the amplitude, we find the partonic cross section at any $\sqrt{\hat{s}}$ is then bounded by⁵

$$\hat{\sigma} < \frac{1}{2^{27} \pi^9} \frac{C_3^2}{\Lambda_g^{2\Delta_g} \Lambda_\gamma^{4\Delta_\gamma}} \hat{s}^{\Delta_g + 2\Delta_\gamma - 1} \left[Q(\Delta_g, \Delta_\gamma) \right]^2 \quad (\text{V.4})$$

⁴ More details will be presented elsewhere.

⁵ Since there are three graphs in the amplitude, each of which has the same bound, there is an overall

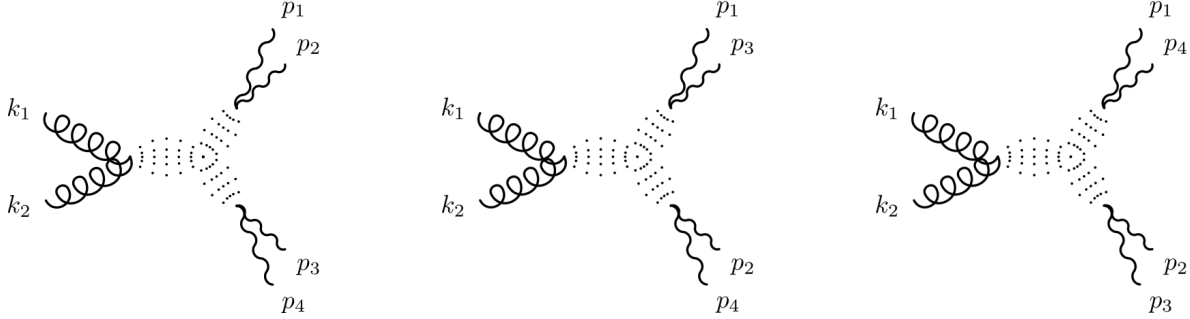


FIG. 2: Feynman diagrams for four photon production at the LHC. The dots represent the conformal three-point function.

with

$$Q(\Delta_g, \Delta_\gamma) = \frac{\Gamma(4 - \frac{\Delta_g}{2} - \Delta_\gamma)}{\Gamma(2 + \frac{\Delta_g}{2} - \Delta_\gamma) [\Gamma(2 - \frac{\Delta_g}{2})]^2} \int_0^1 dx \int_0^{1-x} dy \frac{(xy)^{1-\Delta_g/2} (1-x-y)^{1+\Delta_g/2-\Delta_\gamma}}{\left[xy + \frac{1}{4}(1-x-y)(x+y)\right]^{4-\Delta_g/2-\Delta_\gamma}}. \quad (\text{V.5})$$

Finally, we integrate (V.4) against the gluon-gluon parton luminosity.⁶ At that point we need only substitute the appropriate constraints on Λ_g , Λ_γ and C_3 to obtain the bounds displayed in table II.

B. Commentary

In the table, numbers shown in regular font are those for which only experimental data was used. For these, there is little ambiguity and relatively small uncertainty.⁷ Numbers shown in boldface are those for which unitarity considerations apply for either or both Λ_g or Λ_γ . Theoretical uncertainties are somewhat larger here, as much as a factor of 2. Similar

factor of 3^2 in this expression, canceling the factors of 3 in the phase space integral. The existence of three diagrams appears to have been neglected in [3]. Inclusion would have increased rates, for a given C_d , by a factor of several, but would not much have affected the results quoted in [3], since the change affects both the Tevatron, where experimental bounds were obtained, and LHC, to which these bounds were extrapolated.

⁶ For technical reasons (calculational speed) we have used the outdated CTEQ5M parton distribution functions [19]. As gg luminosities are uncertain at high energies, use of more up-to-date pdfs would shift our answers by up to a few tens of percent. This is comparable to other sources of uncertainty, in particular the extraction of the minimum Λ_g allowed by Tevatron data and unitarity considerations.

⁷ Bounds on the 4γ cross section obtained with purely experimentally-based constraints on the Λ_i are given in Appendix B, in table IV. These bounds remain below a few fb for $\Delta_g + 2\Delta_\gamma$ less than ~ 4.4 .

uncertainties apply for the numbers in *italics*. The relevant uncertainties in these regions are discussed in [1]. It should be noted that it is possible to exceed these bounds as long as one gives up conformal invariance; in this case the rate could be larger, but is not predictable either in magnitude or in its differential distributions.

It appears that the phenomenon suggested in [3] is unobservable at the LHC for smaller values of Δ_g, Δ_γ . For $\Delta_\gamma < 1.7$ the rates are never better than marginal, and other signals of a conformal hidden sector (such as jet-plus-MET or two-photons-plus-MET) may be so much larger that they are easier to observe despite larger backgrounds. The weaker bounds for $\Delta_\gamma > 1.7$ still allow for observable cross-sections, but it is quite possible that there will eventually be bounds on C_3 in this regime. (In the special case studied in [3] where the operators \mathcal{O}_g and \mathcal{O}_γ to which the gluons and photons couple are the same operator, the unitarity constraints of [1] are more powerful, and the numbers on the diagonal at $\Delta_g = \Delta_\gamma = 1.8, 1.9, 2.0$ should be divided by a factor [1] of 33.) We emphasize also that most conformal field theories do not saturate unitarity bounds. We conclude that four-photon production from unparticle interactions is unlikely to be a discovery channel for a conformal hidden sector, or even an observable signal in many cases.

Our work indicates that this direction of research uncovers nothing surprising about conformal field theory. Naively, one would have expected that in a hidden sector with no mass gap, the dominant signals would be in channels with missing momentum, and that the cost to obtain a visible signal would be high, leading only to relatively small and subtle signals.⁸ (This is in contrast to “hidden valleys” [20] where, because of a mass gap in the hidden sector, the visible signatures may easily and naturally dominate.) The suggestion of [3] flies in the face of this expectation. But in fact, the naive intuition appears to be essentially correct.

⁸ Similar naive intuition suggests that two-photon-plus-MET signals are almost always larger than the four-photon signals, because the latter is suppressed by $\Lambda_\gamma^{4\Delta_\gamma}$ while the former is suppressed only by $\Lambda_\gamma^{2\Delta_\gamma}$. It is possible to prove that the four-photon signal can only exceed the digamma-plus-MET signal by a logarithmic enhancement, and this only in extreme circumstances. We therefore suspect that any discovery of a hidden sector coupling to gauge bosons will occur in a MET signal, either with an ISR jet or with two photons.

VI. CONCLUSION

We have considered bounds on couplings of scalar operators built from electroweak bosons to hidden sectors with an exact or approximate conformal invariance above a few GeV. Such “unparticle” sectors are significantly constrained by LEP I and LEP II data on photon-plus-nothing events. We have provided constraints on couplings to both $SU(2)$ and $U(1)$ gauge bosons for $1 \leq \Delta_{\mathcal{O}} \leq 2$. These are particularly powerful at smaller values of $\Delta_{\mathcal{O}}$.

We have also used these results, and those of [1] and [2], to constrain four-photon production at the 14 TeV LHC, dramatically improving the bounds for Δ_γ in the range 1 to 1.7 from of order several pb to far less than 5 fb. For Δ_γ near 2, where the bounds of [2] are not available, the best bounds (a femtobarn if $\mathcal{O}_g = \mathcal{O}_\gamma$, as in [3], and a few tens of femtobarns in the more general case) still come from the methods of [1], due to the lack of a bound on the three-point OPE coefficient from [2]. It seems likely that these bounds will be further strengthened as more is learned about the unitarity constraints on conformal field theory. In particular, the powerful methods of [2] may not yet have been exhausted, and may yet give additional constraints at $\Delta_\gamma > 1.7$.

It is also worth noting that constraints on Λ_g will sharply improve with early data at the LHC. By the time 1 inverse fb of data is obtained at the 14 TeV LHC, it seems likely, if no jet-plus-MET signal is observed, that bounds on Λ_g will improve by a factor of 5 or so relative to the bounds at the Tevatron. This in turn will even further tighten limits on four photon events, long before there is any chance of seeing them. Conversely, if a four-photon signal is observable at the LHC, it seems likely that a jet-plus-MET signal will be detected first.

Acknowledgements

We are grateful to C. Mateuzzi, K. Cranmer, Y. Gershtein, and S. Somalwar for useful discussions. The work of S. Knapen was partially supported by the Belgian American Educational Foundation and the Franqui Foundation. The work of M.J.S. was supported by NSF grant PHY-0904069 and by DOE grant DE-FG02-96ER40959.

Appendix A: Figures

These figures summarize our results for experimental bounds on the strength of CFT coupling to the electroweak gauge bosons. The values Λ_1 and Λ_2 are defined in equation II.1. The plots represent the allowed regions for these variables given constraints from LEP I and LEP II only. The effect of interference between the photon and Z channel for these graphs is very small, and they are drawn for $\delta = 0$, where δ is defined in equation III.6. The graphs include all contributions from equation III.3.

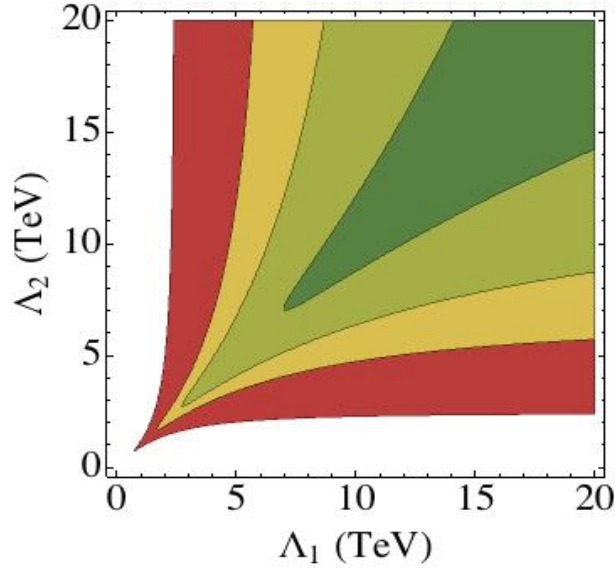


FIG. 3: Plot of 95% CL allowed regions of Λ_1 vs Λ_2 , in units of TeV, from LEP I data for $\delta = 0$. The shaded areas, from largest area to smallest, are the allowed regions for $\Delta = 1.5, 1.35, 1.2, 1.05$.

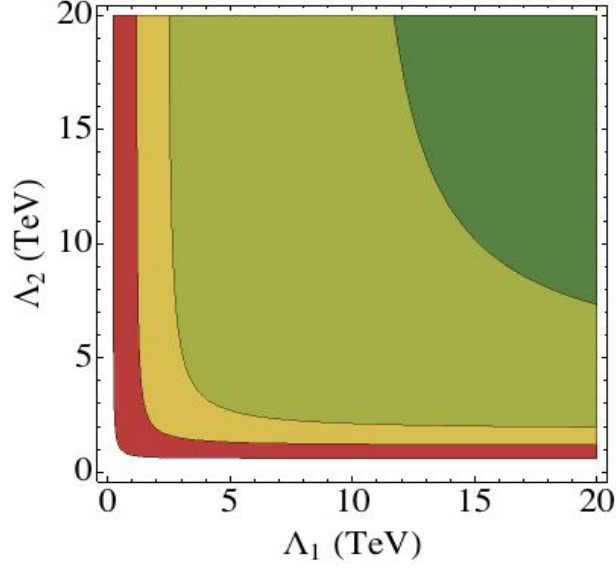


FIG. 4: Plot of 95% CL allowed regions of Λ_1 vs Λ_2 , in units of TeV, from LEP II data for $\delta = 0$. The shaded areas, from largest area to smallest, are the allowed regions for $\Delta = 1.5, 1.35, 1.2, 1.05$.

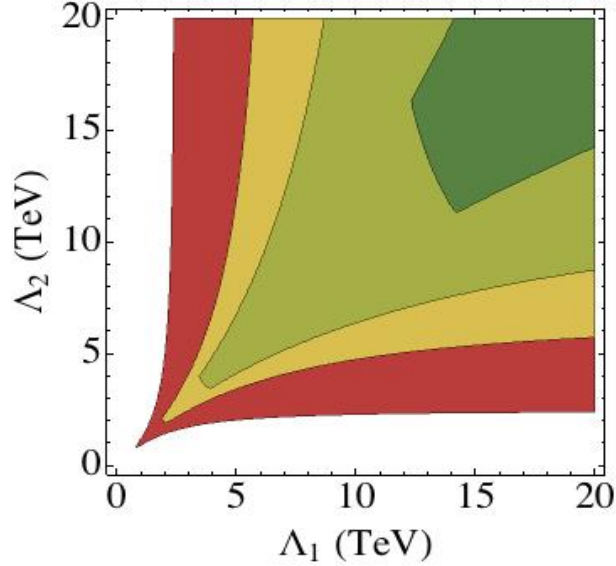


FIG. 5: Combined plot of 95% CL allowed regions of Λ_1 vs Λ_2 , in units of TeV, from both LEP I and LEP II data. This represents the combination of the two previous figures without careful statistical weighting. At the corners of the contours (where both bounds saturate) the true 95% contours would be more rounded than shown. The shaded areas, from largest area to smallest, correspond to $\Delta = 1.5, 1.35, 1.2, 1.05$.

Appendix B: Bounds without unitarity argument

In the table below are shown the bounds on $gg \rightarrow \gamma\gamma\gamma\gamma$ that would be obtained with our methods using only experimental bounds on Λ_g and Λ_γ and the unitarity bounds on the conformal three-point function coefficient C_3 from [2]. No theoretical assumptions go into these bounds, so they are particularly robust.

| $\Delta_g \setminus \Delta_\gamma$ | 1.05 | 1.1 | 1.2 | 1.3 | 1.4 | 1.5 | 1.6 | 1.7 |
|------------------------------------|----------------------|----------------------|----------------------|-------|-------|------|-------|--------|
| 1.05 | 2.7×10^{-6} | 2.7×10^{-5} | 4.8×10^{-4} | 0.010 | 0.093 | 0.62 | 6.4 | 110. |
| 1.1 | 5.2×10^{-6} | 5.2×10^{-5} | 6.7×10^{-4} | 0.014 | 0.13 | 0.89 | 9.2 | 110. |
| 1.2 | 1.5×10^{-5} | 1.4×10^{-4} | 1.3×10^{-3} | 0.029 | 0.37 | 2.4 | 19. | 180. |
| 1.3 | 3.7×10^{-5} | 3.1×10^{-4} | 4.8×10^{-3} | 0.058 | 0.76 | 4.9 | 40. | 370. |
| 1.4 | 9.0×10^{-5} | 7.8×10^{-4} | 9.6×10^{-3} | 0.12 | 1.6 | 10. | 85. | 800. |
| 1.5 | 2.5×10^{-4} | 2.0×10^{-3} | 0.030 | 0.35 | 3.2 | 21. | 210. | 1600. |
| 1.6 | 6.1×10^{-4} | 5.2×10^{-3} | 0.060 | 0.71 | 6.6 | 44. | 520. | 4000. |
| 1.7 | 1.9×10^{-3} | 0.014 | 0.17 | 1.9 | 18. | 110. | 1100. | 9600. |
| 1.8 | 4.1×10^{-3} | 0.023 | 0.24 | 3.9 | 46. | 230. | 2600. | 23000. |
| 1.9 | 7.3×10^{-3} | 0.040 | 0.49 | 6.0 | 77. | 600. | 6500. | 63000. |

TABLE IV: Bounds, in fb, on 4 photon production at the LHC (14 TeV), using only constraints from experiment and internal consistency of the conformal field theory. No unitarity arguments are used here in constraining Λ_g or Λ_γ . There is no bound for $\Delta_\gamma > 1.7$, since no bound on C_3 is known there.

Appendix C: Detail of analysis

At both LEP I and LEP II, the highest signal-to-background ratio is found for large photon energies. The only significant source of standard model background in this regime is $\nu\bar{\nu}\gamma$ production, which falls quickly with rising photon energy [21]. As mentioned before, the unparticle signal is peaked at higher photon energy.

Optimal values for the photon energy cut were found using the following method. For any potential value of the cut energy E_{cut} , the bound on Λ_Z or Λ_γ was calculated for any number

n of observed photon events with energy above the cut. These bounds were then averaged over n , using a Poisson distribution for n assuming the only source is the background. The value of E_{cut} that produces the strongest average expected bound on Λ_Z or Λ_γ via this method is then used as the energy cut, following [13].

For LEP I, we can reproduce reasonably well the shape of each experiment's Monte Carlo simulation of background with the background model [21]. We fit the normalization to account for each experiment's efficiency. An additional complication was that L3 had a larger angular acceptance than OPAL, DELPHI and ALEPH. For the purpose of being conservative, we only considered the signal in the wedge that all four detectors have in common, but took into account the background for the entire L3 detector.

The cut energies for different values of Δ were calculated to the nearest 0.2 GeV, maximizing the expected bound on Λ_Z , and can be found in table V. The signal efficiencies for these cuts range from 0.98 for Δ close to 1 to 0.74 for Δ close to 2.

In the case of LEP II, the background model is less clear-cut. The background in L3 and ALEPH is very small, and the resolution of the plots is insufficient to make a reliable estimate. We therefore chose to omit any background from L3 and OPAL in our analysis. For OPAL and especially DELPHI, the background is more significant. However, because of the rather low resolution of DELPHI's inner detector wedge (HPC), we cannot reproduce the shape of DELPHI's Monte Carlo with the background model of [21]. Instead we used a more general fit function with three fit parameters to model the background in OPAL and DELPHI.

Furthermore, DELPHI is the only experiment that has separate plots available for the different segments of its detector. Since the signal is rather flat in $\cos\theta$ and the background is peaked in the forward region, we only consider DELPHI's inner wedge to increase the signal to background ratio. As DELPHI's resolution is inferior compared to the other three experiments, it has some background events leaking into the signal region, resulting from the smearing of the Z-peak. These events significantly weaken our bound for values of Δ close to 2.

To calculate the cuts, the same analysis was performed as was done for LEP I, but now in terms of missing mass. The cut on the missing mass was calculated to the nearest 1.0 GeV, maximizing the expected bound on Λ_γ , and can be found in table V.

To determine the bounds at 95% confidence level, the following equation was used, from

| Δ | 1 | 1.05 | 1.1 | 1.2 | 1.3 | 1.4 | 1.5 | 1.6 | 1.7 | 1.8 | 1.9 | 2 |
|------------------------|------|------|------|------|------|------|------|------|------|------|------|------|
| E_{cut} (GeV) | 43.8 | 42.0 | 40.8 | 39.0 | 37.8 | 36.6 | 35.8 | 34.8 | 34.0 | 33.2 | 32.4 | 31.6 |

TABLE V: The photon energy cut for the different values of Δ for LEP I.

| Δ | 1 | 1.05 | 1.1 | 1.2 | 1.3 | 1.4 | 1.5 | 1.6 | 1.7 | 1.8 | 1.9 | 2 |
|------------------------|----|------|-----|-----|-----|-----|-----|-----|-----|-----|-----|----|
| M_{cut} (GeV) | 15 | 22 | 26 | 30 | 33 | 35 | 37 | 39 | 41 | 43 | 45 | 48 |

TABLE VI: The missing mass cut for the different values of Δ for LEP II.

[13]

$$(1 - 0.95) \sum_{n=0}^{n_0} \frac{\mu_B^n}{n!} = e^{-N} \sum_{n=0}^{n_0} \frac{(\mu_B + N)^n}{n!}, \quad (\text{C.1})$$

where μ_B is the expected number of background events, n_0 is the number of observed events, and N is the 95% CL upper limit on the expected number of signal events. Note that if $n_0 = 0$, corresponding to no observed events, then $N = 2.99$ independent of the number of expected background events.

At LEP I, none of the experiments observed any events with energies above the cuts. The bound was imposed by integrating the cross section III.8 above the appropriate energy cut, within the angular wedge that all four detectors shared ($\cos \theta < 0.7$), and accounting for the various detector efficiencies and luminosities. The calculation was performed at each value of \sqrt{s} used by the experiments,⁹ and summed over all values, accounting for the various efficiencies and luminosities.

At LEP II, some events were observed that passed the missing mass cuts. The events were counted by hand from the graphs in [14–17]. As in LEP I, the integrated cross section was bounded to the appropriate value computed from equation C.1. Again, the calculation was performed at each value of \sqrt{s} used by the experiments, and summed over all values, accounting for the various efficiencies and luminosities. When computing the expected signal, we have been conservative by only accounting for angular acceptance that all detectors have

⁹ We are thankful to K. Cranmer from L3 for providing us with this additional information.

in common with DELPHI's inner wedge ($\theta < 45^\circ$).

-
- [1] A. Delgado and M. J. Strassler, *A Simple-Minded Unitarity Constraint and an Application to Unparticles*, Phys. Rev. **D81** (2010) 056003, [arXiv:0912.2348 \[hep-ph\]](#)
 - [2] F. Caracciolo and S. Rychkov, *Rigorous Limits on the Interaction Strength in Quantum Field Theory*, [arXiv:0912.2726 \[hep-th\]](#)
 - [3] J. L. Feng, A. Rajaraman and H. Tu, *Unparticle self-interactions and their collider implications*, Phys. Rev. **D77** (2008) 075007, [arXiv:0801.1534 \[hep-ph\]](#)
 - [4] H. Georgi, *Unparticle physics*, Int. J. Mod. Phys. **A25** (2010) 573–586
 - [5] B. Grinstein, K. A. Intriligator and I. Z. Rothstein, *Comments on Unparticles*, Phys. Lett. **B662** (2008) 367–374, [arXiv:0801.1140 \[hep-ph\]](#)
 - [6] A. E. Nelson, M. Piai and C. Spitzer, *Protecting unparticles from the MSSM Higgs sector*, Phys. Rev. **D80** (2009) 095006, [arXiv:0905.0503 \[hep-ph\]](#)
 - [7] K. Cheung, W.-Y. Keung and T.-C. Yuan, *Collider Phenomenology of Unparticle Physics*, Phys. Rev. **D76** (2007) 055003, [arXiv:0706.3155 \[hep-ph\]](#)
 - [8] B. Field, S. Dawson and J. Smith, *Scalar and pseudoscalar Higgs boson plus one jet production at the LHC and Tevatron*, Phys. Rev. **D69** (2004) 074013, [arXiv:hep-ph/0311199](#)
 - [9] **DELPHI** Collaboration, P. Abreu *et al.*, *Search for new phenomena using single photon events in the DELPHI detector at LEP*, Z. Phys. **C74** (1997) 577–586
 - [10] **L3** Collaboration, M. Acciarri *et al.*, *Search for new physics in energetic single photon production in e^+e^- annihilation at the Z resonance*, Phys. Lett. **B412** (1997) 201–209
 - [11] **OPAL** Collaboration, R. Akers *et al.*, *Measurement of single photon production in e^+e^- collisions near the Z^0 resonance*, Z. Phys. **C65** (1995) 47–66
 - [12] **ALEPH** Collaboration, D. Buskulic *et al.*, *A Direct measurement of the invisible width of the Z from single photon counting*, Phys. Lett. **B313** (1993) 520–534
 - [13] S. I. Bityukov and N. V. Krasnikov, *Confidence intervals for the parameter of Poisson distribution in presence of background*, ArXiv Physics e-prints (Sept., 2000) [arXiv:physics/0009064](#)
 - [14] **DELPHI** Collaboration, J. Abdallah *et al.*, *Photon events with missing energy in e^+e^-*

- collisions at $s^{**}(1/2) = 130\text{-GeV}$ to 209-GeV* , Eur. Phys. J. **C38** (2005) 395–411,
arXiv:hep-ex/0406019
- [15] **ALEPH** Collaboration, A. Heister *et al.*, *Single photon and multiphoton production in e^+e^- collisions at \sqrt{s} up to 209-GeV* , Eur. Phys. J. **C28** (2003) 1–13
- [16] **L3** Collaboration, P. Achard *et al.*, *Single photon and multiphoton events with missing energy in e^+e^- collisions at LEP*, Phys. Lett. **B587** (2004) 16–32, arXiv:hep-ex/0402002
- [17] **OPAL** Collaboration, G. Abbiendi *et al.*, *Photonic events with missing energy in e^+e^- collisions at $s^{**}(1/2) = 189\text{-GeV}$* , Eur. Phys. J. **C18** (2000) 253–272,
arXiv:hep-ex/0005002
- [18] **CDF** Collaboration, T. Aaltonen *et al.*, *Search for large extra dimensions in final states containing one photon or jet and large missing transverse energy produced in $p\bar{p}$ collisions at $\sqrt{s} = 1.96\text{-TeV}$* , Phys. Rev. Lett. **101** (2008) 181602, arXiv:0807.3132 [hep-ex]
- [19] **CTEQ** Collaboration, H. L. Lai *et al.*, *Global QCD analysis of parton structure of the nucleon: CTEQ5 parton distributions*, Eur. Phys. J. **C12** (2000) 375–392,
arXiv:hep-ph/9903282
- [20] M. J. Strassler and K. M. Zurek, *Echoes of a hidden valley at hadron colliders*, Phys. Lett. **B651** (2007) 374–379, arXiv:hep-ph/0604261
- [21] G. Barbiellini *et al.*, *NEUTRINO COUNTING*, Presented at Workshop on Z Physics at LEP